Controlled structuring of binary hard-disk mixtures via a periodic, external potential

K. Franzrahe* and P. Nielaba
Fachbereich Physik, Universität Konstanz, Postfach 692,78457 Konstanz, Germany
(Received 4 March 2009; published 28 May 2009)

Ordering phenomena on surfaces or in monolayers can be successfully studied by model systems as binary hard-disk mixtures, the influence of a substrate being modeled by an external potential. For the field-free case the thermodynamic stability of space-filling lattice structures for binary hard-disk mixtures is studied by Monte Carlo computer simulations. As these structures prove to be thermodynamically stable only in high pressure environments, the phase behavior of an equimolar binary mixture with a diameter ratio of $\sigma_B/\sigma_A=0.414$ exposed to an external, one-dimensional, periodic potential is analyzed in detail. The underlying ordering mechanisms and the resulting order differ considerably, depending on which components of the mixture interact with the external potential. The simulations show that slight deviations in the concentration of large particles x_A or the diameter ratio σ_B/σ_A have no impact on the occurrence of the various field-induced phenomena as long as the mixture stays in the relevant regime of the packing fraction η. Furthermore the importance of the commensurability of the external potential to the $S_1(AB)$ square lattice for the occurrence of the induced ordering is discussed.

DOI: 10.1103/PhysRevE.79.051505 PACS number(s): 64.75.Gh, 64.70.D−, 61.20.Ja, 82.70.Dd

I. INTRODUCTION

Soft matter with its structural and elastic properties offers an attractive route to the design of new materials. The importance of structured surfaces or monolayers lies in their promising, versatile technical applicability. Examples are antireflection surfaces, optical storage media or the usage in template-directed colloidal crystallization, the resulting three-dimensional colloidal crystals being, e.g., of interest due to their tailored photonic band gaps [1–5]. The physics of surfaces and adsorbed monolayers has attracted a lot of interest in this context. In theoretical studies two-dimensional systems are often used as a model, the interactions with substrates being conveniently modeled by external fields. The experimental counterpart, two-dimensional systems of colloidal suspensions, has been studied extensively in the last decades. They offer direct access to real space data via laser scanning microscopy [6,7], an excellent control over the colloidal interactions and easy tunability of the substrate potential in its shape and strength, as it is modeled, e.g., by interference patterns of laser beams. A close interplay between experiments, analytic theory, and computer simulations helped to shed light on such fundamental questions of statistical physics as the nature of melting in two dimensions with [8–22] and without [23–28] the influence of external fields. The interaction of monodisperse, two-dimensional systems with one-dimensional, periodic light fields lead to the discovery of complex phase behavior as for example laser induced freezing (LIF) [8,9,13] and laser induced melting (LIM) [12,14].

Particularly with respect to the interest in complex, two-dimensional structures for the design of new materials and the rich phase behavior resulting from the interaction of monodisperse systems with simple external light fields, questions arise, as to what complex, periodic structures binary mixtures might assemble in, and what influence an interaction with simple external light fields has on the phase behavior of such mixtures. The focus of this paper is in particular on the differences in the induced ordering and ordering mechanisms that result from the various possible interaction scenarios with the external potential in a mixture. Binary hard-disk mixtures are chosen as a model system for the clarification of these questions. Hard-disks are neither selective in the choice of the type of next-neighbor particles nor in the number of next-neighbor particles. Therefore the model system is ideal to show what ordering can result solely from geometric constraints due to the diameter ratio σ_B/σ_A of the components of the mixture and due to the concentration of the mixture. These characteristics make them also a good model for the ground state of atomic systems with short range interactions.

The paper is organized as follows. In Sec. II the model system is introduced and details of the computer simulations are given. Here also definitions for various parameters used in the analysis of structural order are given. In the following sections results are presented and discussed. The focus lies first on the thermodynamic stability of space-filling lattice structures, as they are proposed by Likos and Henley [29] in the limit $T\rightarrow 0$. The presented Monte Carlo simulations in the NpT ensemble show that complex lattice structures can only exist at high hydrostatic pressure as thermodynamically stable phases. Such high external pressure will inevitably lead to buckling in surface structuring applications. An attractive alternative to induce order in such systems offers the controlled manipulation of colloidal systems by external fields. In what follows therefore systematic studies via Monte Carlo simulations in the NVT ensemble of a bidisperse, 50% hard-disk mixture with diameter ratio $\sigma_B/\sigma_A=0.414$ subjected to an external, one-dimensional, periodic light field are presented. The underlying ordering mechanisms leading to laser induced phenomena [30], as laser-induced demixing (LID), fissuring and laser induced coexistence of a square lattice phase with a fluid phase as well as their dependence on the details of the interaction with the

*kerstin.franzrahe@uni-konstanz.de

 ©2009 The American Physical Society

external field, diameter ratio, concentration of the binary mixture, and commensurability of the external potential are discussed in detail.

II. MODEL AND METHODS

We model the analyzed, binary, two-dimensional mixtures by $N=N_A+N_B$ hard-disks. The diameter of the larger component of the mixture is set to $\sigma_A=1$ in all simulations. All lengths are measured in units of σ_A. The packing fraction of the mixture is defined as $\eta=\varrho^*\pi(N_A\sigma_A^2+N_B\sigma_B^2)/(4N)$, where $\varrho^*=\varrho\sigma_A^2$ is the dimensionless number density. The concentration of large particles in the mixture is given by $x_A=N_A/N$. The mixtures under study are additive mixtures. The pair potential is given by

$$\phi(r_{ij})=\begin{cases}\infty & \text{if } r_{ij}\leq\sigma_{ij}\\ 0 & \text{if } r_{ij}>\sigma_{ij}.\end{cases}$$

Here $\sigma_{ij}=\sigma_A$ for $i,\ j\in N_A$, $\sigma_{ij}=\sigma_B$ for $i,\ j\in N_B$ and $\sigma_{ij}=(\sigma_A+\sigma_B)/2$ for $i\in N_A$ and $j\in N_B$ or vice versa. Information on the equilibrium phase behavior of these mixtures is obtained via Monte Carlo computer simulations. Periodic boundary conditions are employed in all simulations. Besides the standard Metropolis algorithm [31] a cluster move by Lue [32] is employed.

Simulations in the NpT ensemble were used for testing the thermodynamic stability of given lattice structures. Here the simulation volume can fluctuate (although shearing the simulation box was not attempted). In these studies suggested space-filling lattice structures for various binary mixtures [29] were set up with $N\approx1000$. Simulations were run starting from a high, hydrostatic external pressure $p^*=p\sigma_A^2/k_BT$ and lowering it in successive runs. The resulting change in packing fraction η with pressure p^* was monitored. After equilibrating the system for 10^6 Monte Carlo steps (MCS), data were taken for another 2×10^6 MCS.

The influence of a modulated external field was analyzed by Monte Carlo simulations in the NVT ensemble. In these simulations additional nonlocal moves are attempted with particle displacements, which are integer multiples of the potential wavelength. The simulation box is set up to be slightly rectangular with $L_x/L_y\approx1.178$ and $N=1848$ for these simulations. This choice allows not only a box-spanning square lattice to form, but also a box-spanning monodisperse triangular lattice of the larger component can develop. Controlled, field-induced ordering was analyzed in a $x_A=50\%$ mixture with diameter ratio $\sigma_B/\sigma_A=0.414$. In such a mixture closed packing is achieved by a $S_1(AB)$ lattice structure. After equilibrating the system for 10×10^6 Monte Carlo steps (MCS) the simulations were run for another 10×10^6 MCS and data were taken. The external field is modeled by a one-dimensional, periodic potential:

$$V(\vec{r})=V_0\sin(\vec{K}\cdot\vec{r}).$$

The wave vector $\vec{K}=\frac{4\pi}{a}(1,0)$ is set to be commensurate to the $S_1(AB)$ lattice with a commensurability ratio $p=|\vec{K}|/|\vec{G}|=2$. This implies a wavelength $\lambda=2\pi/|\vec{K}|=1/\sqrt{2\varrho^*}$. The amplitude of the external potential is given in units of k_bT, i.e., $V_0^*=V_0/k_BT$. The resulting energy landscape for particles interacting with the external field is shown schematically in Fig. 1. For a binary mixture one needs to distinguish three different, possible interaction scenarios: (i) only the small component of the mixture interacts with the external field; (ii) both components of the mixture interact with the external field; (iii) only the large component of the mixture interacts with the external field.

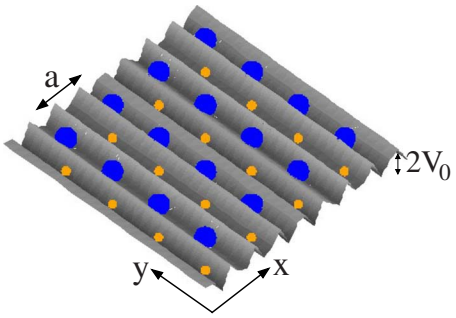

FIG. 1. (Color online) Schematic drawing of the energy landscape for particles interacting with the external field, which is commensurate to the $S_1(AB)$ square lattice with a commensurability ratio $p=2$, for an equimolar, binary mixture with diameter ratio $\sigma_B/\sigma_A=0.414$.

In experimental setups the external potential is often generated by the interference pattern of two laser beams. If the particle size is not negligible in comparison to the fringe spacing of the interference pattern, the oscillatory part of the external potential picks up a fringe wave vector $\vec{K}$ and particle size-dependent prefactor [9,33]. Thus e.g., an appropriate choice of wave vector $\vec{K}$ and particle diameters σ_A and σ_B can be used in the experimental realization of the three different interaction scenarios of a binary mixture with such an external field [33].

Voronoi diagrams are used to visualize structural order in the configurations. Quantitative information on the type of order induced can be obtained by calculating the shape factor $\zeta=\frac{C^2}{4\pi A}$ of the Voronoi cells [34]. It is a measure, which compares the circumference C of the Voronoi cell with its surface area A. Thus a circular structure has a shape factor of $\zeta=1$, while all cells deviating from this result in $\zeta>1$. In these studies the shape factor is used to identify square ($\zeta=1.273$) and regular, hexagonal ($\zeta=1.1026$) structures. The probability distributions of the shape factor $P(\zeta)$ are calculated from all Voronoi diagrams obtained from the analyzed configurations within a simulation run. They are used to determine phase boundaries. A typical probability distribution $P(\zeta)$ for the fluid phase is shown in Fig. 2. The inset shows a typical Voronoi diagram of a fluid configuration. Although the Voronoi diagram shows a lot of cells with irregular rectangular (black), pentagonal (dark gray, color online: blue) or hexagonal (light gray, color online: orange) structure, no crystallites with *regular* cells are present. Therefore $P(\zeta)$ is a broad distribution with no significant maxima. The change in the structural ordering of a system due to the interaction with an external potential can be analyzed by calculating the change in the probability distributions of the shape factor $\Delta P(\zeta)=P(\zeta;V_0^*)-P(\zeta;V_0^*=0.0)$.

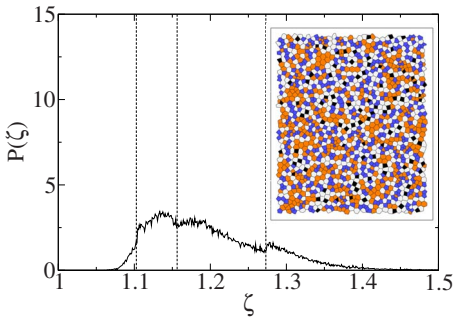

FIG. 2. (Color online) The probability distribution of the shape factor $P(\zeta)$ for an equimolar binary mixture with diameter ratio $\sigma_B/\sigma_A=0.414$ in the fluid phase at $\varrho^*=1.6$ and $V_0^*=0$. The inset shows a typical Voronoi diagram of a fluid configuration. Voronoi cells are colored according to their structure: rectangular black, pentagonal dark gray (blue) and hexagonal light gray (orange). All other structures are plotted in white.

An alternative way to quantify order in the configurations is the use of rotational order parameters Ψ_m. Rotational order parameters are defined on the interval [0, 1]. In case the system has a m-fold symmetry axis $\Psi_m=1$. The local rotational order is calculated by $\Psi_{m,j}=\frac{1}{N_b}\sum_{k=1}^{N_b}e^{i(m\theta_{kj})}$. Here θ_{kj} is the angle between the line through particles j and k and the x axis and N_b is the number of next neighbors taken into account in the analysis of local order. The global rotational order of the system is obtained from $\Psi_m=|\frac{1}{N}\sum_{j=1}^{N}\Psi_{m,j}|$. An analysis of the rotational order of the sublattice of the larger component of the mixture searching for fourfold or sixfold rotational symmetry axes is used to identify square and/or hexagonal ordered structures induced by the external field. Square lattice structures can also be identified by calculating Ψ_8 taking into account *all* particles in the mixture. Due to the occurrence of a fissuring regime, the probability distributions $P(\Psi_m)$ develop asymmetric tails, which hampers an analysis via Binder cumulants.

In addition specific order parameters S_B and S_A are defined [30]. These capture the characteristic properties of the observed phases, especially the fissuring regime. They are derived from the order parameter for nematic liquid crystals (e.g., [35]), as upon the onset of fissuring dimers of small particles form that can be oriented along the potential minima. Therefore S_B is constructed to take on values not equal zero as soon as such dimers appear. The local order parameter $S_{B,j}$ is defined as

$$S_{B,j}=\begin{cases}0 & \text{if } Z_B=0\\ \dfrac{1}{Z_B}\displaystyle\sum_{k=1}^{Z_B}\dfrac{3(\cos\,\theta_{jk})^2-1}{2} & \text{if } Z_B\neq 0,\end{cases}$$

with Z_B the number of next neighbors of a small colloid j, which are also small colloids. All small colloids within a cutoff radius $r_c=\lambda$ of j are considered as next neighbors. The angle θ_{jk} measures the orientation of the connection line between j and its next neighbor with respect to the potential minima. The global order parameter is obtained by evaluating the average over N_B, the number of small particles with $Z_B\neq 0$, i.e.,

$$S_B=\frac{1}{N_B}\sum_{j=1}^{N_B}S_{B,j}.$$

S_B is defined on the interval $[-0.5,1]$. Dimers aligned with the potential minima of the external field result in $S_B=1$, while those oriented perpendicular to the potential minima result in $S_B=-0.5$. In case of a coexistence of the $S_1(AB)$ square lattice with a fluid phase the peaks in the probability distribution $P(S_B)$ at $S_B=1$ and $S_B=-0.5$ disappear. S_A is the analogous order parameter for the large particles. Here the cutoff radius, within which next-neighbor particles lie, is set to $r_c=1.3\sigma_A$. In addition the distance between next-neighbor particles in x direction must be smaller than λ. In the ordered $S_1(AB)$ square lattice phase $P(S_A)$ exhibits a deltalike peak at $S_A=1$. A loss in the alignment of dimers of the large component with the orientation of the potential minima shifts the peak in $P(S_A)$ to lower values. From the analysis of $P(S_A)$ and $P(S_B)$ phase boundaries are determined.

III. THERMODYNAMIC STABILITY OF BINARY LATTICE STRUCTURES

An analysis of space-filling packings for binary, hard-disk mixtures in the $T\rightarrow 0$ limit by Likos and Henley [29] resulted in the prediction of a detailed phase diagram. In these studies the constant hydrostatic pressure acting on the system is set to $p=1$ and contributions to the free energy from entropy are ignored in the calculation. Thus a ground-state phase diagram is obtained. The method by which the lattice structures given in the phase diagram are selected relies on a maximization of the packing fraction η. In certain regimes the packing fraction of lattice-gas structures, random tilings, and coexistence between lattice structures is the same. For these cases Likos and Henley [29] argue that the preferred structure is the one with the least order due to its higher entropy for $T>0$. From these results one expects a large number of lattice structures to exist in two-dimensional systems. Thus the question arises of how difficult it is to obtain such structures and how stable these structures are. In the studies presented here, the thermodynamic stability of various of the suggested pure phases is tested by use of Monte Carlo simulations in the NpT ensemble

For equimolar, binary mixtures two possible lattice structures are suggested by Likos and Henley [29]. In the interval $\sigma_B/\sigma_A\in[0.392,0.414]$ a $S_1(AB)$ square lattice structure and a $H_2(AB)$ structure in the intervals $\sigma_B/\sigma_A\in(0.414,0.438]$ and $\sigma_B/\sigma_A\in[0.627,0.646]$. $S_1(AB)$ square lattice structures were set up and simulated for $\sigma_B=0.392$, 0.396, 0.400, and 0.414. Figure 3(a) shows the packing fraction η as a function of decreasing pressure p^*, as it is obtained from simulations. The discontinuous decrease in η signifies the transition from the ordered phase to the fluid phase. The square lattice structure is stable for $p^*\geq 32$ for all simulated mixtures. $H_2(AB)$ lattice structures were set up and simulated for $\sigma_B=0.627$, 0.638, 0.640, and 0.646. The packing fraction as a function of decreasing pressure p^* is plotted in Fig. 3(b). This lattice

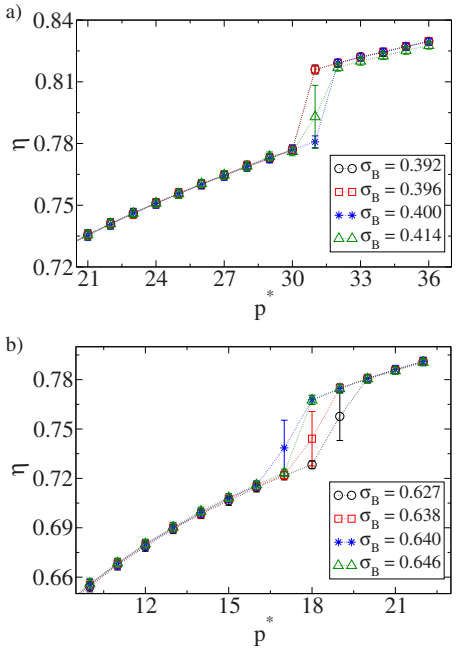

FIG. 3. (Color online) The packing fraction η as a function of decreasing pressure p^* in an equimolar binary mixture. Two different lattice structures are tested for their stability: (a) the $S_1(AB)$ square lattice for various mixtures with $\sigma_B/\sigma_A \in [0.392, 0.414]$. (b) The $H_2(AB)$ lattice for mixtures with $\sigma_B/\sigma_A \in [0.627, 0.646]$.

structure stays stable in systems with $p^* \geq 20$ for the analyzed mixtures. In Fig. 3(b) the stability of the $H_2(AB)$ structure increases as the diameter of the smaller particles σ_B gets larger. This can be understood, if one recalls that as $\sigma_B \to 1$ the $H_2(AB)$ structure transforms directly into the monodisperse triangular lattice structure. In comparison a higher external pressure is needed in order to stabilize a $S_1(AB)$ square lattice structure in the equimolar mixture.

An overview of the simulated binary mixtures is given in Fig. 4. Structures, for which a pressure regime, in which the structures stay stable, could be identified, are marked by crosses (green). For the mixture with $x_B = 4/5$ marked by a triangle (blue) the lattice structure was not stable within the simulated pressure regime of $p^* \leq 200$. For illustration sketches of the studied lattice structures are shown in Fig. 4. Also given are the packing fraction η and the pressure p^*, above which *all* of the simulated mixtures were found to be stable for the given lattice structures. Figure 4 shows that the more a given lattice structure deviates from the triangular, monodisperse lattice the higher the hydrostatic pressure needed to stabilize it. The simulations show that the complex, space-filling lattice structures for binary hard-disk mixtures are high pressure phases. This makes it difficult to observe such structures in experimental set ups, as by increasing the pressure within the surface the probability that the monolayer will escape into the third dimension by buckling will also increase. These findings show clearly the importance of the search for alternative ways to stabilize or induce the formation of ordered structures in two-dimensional, binary mixtures. One promising approach is the use of external fields.

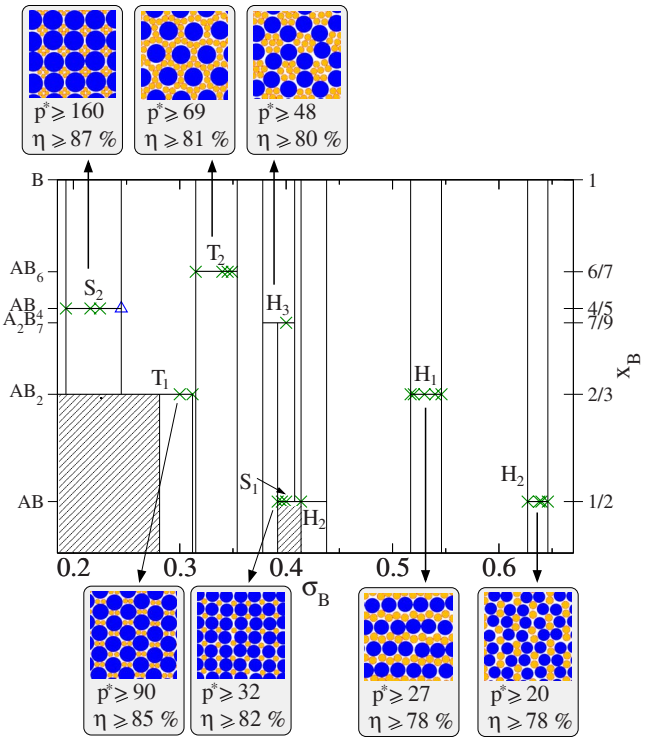

FIG. 4. (Color online) Overview of analyzed lattice structures for binary hard-disk mixtures. Structures for which a pressure regime, in which the structures stay stable, could be identified are marked by crosses (green). For the mixture marked by a triangle (blue) the lattice structure was not stable within the simulated pressure regime of $p^* \leq 200$. Also given are the packing fraction η and the pressure p^* above which *all* of the simulated mixtures for the given lattice structure were found to be stable.

IV. CONTROLLED STRUCTURING BY EXTERNAL FIELDS

Exposing a monodisperse two-dimensional fluid to an external field, which is modulated periodically in one dimension, one observes a modulation in the density according to the imposed modulation. Such a fluid phase is called a modulated liquid (ML). In addition to this direct response to the external field such systems are known to show a surprisingly complex phase behavior. E.g., depending on the choice of parameters defining the system, reentrant LIF and LIM transitions can occur. As the amplitude of the modulated external field is increased the system freezes into a locked floating solid. A further increase in the amplitude results in a strong confinement of the particles within the minima of the external field and an increase in fluctuations along these minima. This leads to an uncoupling of particles in adjacent minima and therefore a reentrant melting into the modulated liquid. These laser induced phenomena in monodisperse systems have been studied extensively in experiments [8–10,13,14], computer simulations [12,18–22], and various analytic theories [8,11,15–17] over the last decades. For a review on these phenomena in monodisperse systems see [17] and reference therein. Both the laser induced freezing and the lattice structure of the resulting locked floating solid, as well as the details of the reentrance into the modulated liquid depend

strongly on the choice of commensurability ratio p and the choice of interaction potential of the particles. Further interesting laser induced phenomena, such as laser induced condensation, are predicted to occur in three-dimensional colloid-polymer mixtures, when they are exposed to a periodically modulated external field [36].

In the studies presented in this paper, we focus on the controlled ordering of two-dimensional, binary mixtures. By exposing these mixtures to similar external fields as in the monodisperse studies, we extend these studies to a more general situation and retain at the same time the possibility for a direct comparison of the order inducing mechanisms at work. The focus is thus on the question of how the addition of another length scale into the system influences the intricate competition between adsorbate-adsorbate and adsorbate-substrate interactions and whether such a simple external field will suffice for a controlled structuring of the monolayer. As has been discussed in detail in [30,37] for the case that only the smaller component of the mixture interacts with the external field, laser induced phenomena such as LID and a laser induced coexistence could be identified and the interaction with the substrate completely changes the miscibility of the binary mixture.

In this paper, we show that the underlying ordering mechanisms in a binary mixture exposed to an external field differ significantly depending on which components interact with the external potential. To this end we compare the occurring phases (ML, LID, fissuring, and LIF) and the resulting phase diagrams for the possible coupling scenarios for the components of the mixture to the external field. In addition the influence the relative strength of the coupling of the different components of the mixture to the external field has on the ordering is studied. These differences are discussed in detail, as well as the influence of incommensurability of the periodicity of the external field and alterations in the type of mixture due to deviations from equimolar mixtures or from the diameter ratio $\sigma_B/\sigma_A=0.414$ of the components.

A. Modulated liquid

At low number densities ϱ^* the external field induces a variation in the density according to the external periodicity in the liquid phase. The characteristics of the resulting modulated liquid vary for the three analyzed couplings of the components of the mixture to the external potential. Nevertheless all three scenarios show an *induced* structural crossover. Structural crossover has been predicted to occur in binary mixtures by Grodon *et al.* [38,39] and has been recently observed experimentally [40]. As discussed in detail in [30] a structural crossover is induced for the case that only the small component interacts with the external field. For $V_0^*=0$ the large particles in the mixture form a spanning network. The dominating wavelength in the asymptotic oscillations in the pair correlation functions $g_{AA}(r)$ and $g_{BB}(r)$ is therefore set by the radius of the large particles. Due to the coupling to the external potential the wavelength of the exponentially damped oscillations in the pair correlation functions changes from approximately $\sigma_A/2$ in the field free case to $\lambda/2$ in the modulated liquid.

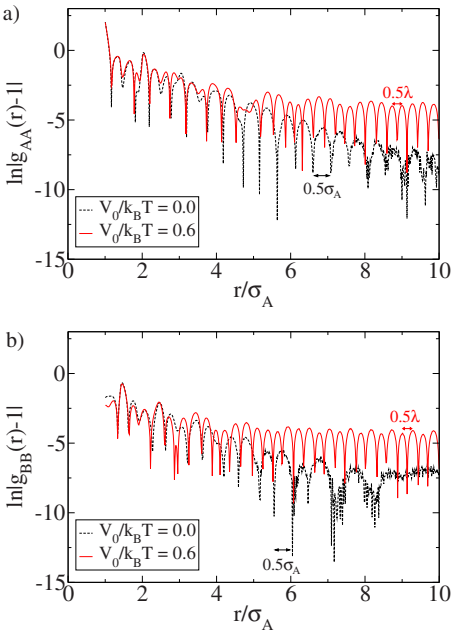

FIG. 5. (Color online) Comparison of the total pair correlation functions (a) $h_{AA}(r)$ and (b) $h_{BB}(r)$ of an equimolar mixture with $\sigma_B/\sigma_A=0.414$ exposed to an external, periodic potential at $\varrho^*=1.60$. Shown is the case when both components of the mixture interact with the external potential.

Figure 5 shows the total correlation functions $h_{BB}(r)$ and $h_{AA}(r)$ for the case that both components interact with the external potential. As in the case that only the small component interacts with the external field [30], both correlation functions show an induced structural crossover. But, while the system at $\varrho^*=1.6$ is still in the modulated liquid phase for an amplitude of the external potential of $V_0^*=2.1$ for the case of an exclusive interaction of the small component of the mixture with the external potential, this is no longer true, if the large component interacts with the external potential as well. Therefore Fig. 5 shows the total correlation functions at $V_0^*=0.6$, where the system is still in the modulated liquid phase, as can be seen in the phase diagram for this scenario of interaction of the components of the mixture with the external potential in Fig. 10.

In contrast to this a coupling of solely the large component to the external field suffices not to imprint the periodicity of the external potential on the total correlation functions of the component *not* interacting directly with the external potential, i.e., $h_{BB}(r)$. Figure 6 shows the total correlation functions $h_{BB}(r)$ and $h_{AA}(r)$ for this situation. For $h_{AA}(r)$ in Fig. 6(a) a structural crossover to a dominant wavelength of $\lambda/2$ in the asymptotic oscillations is evident. This wavelength cannot be discerned in $h_{BB}(r)$, as Fig. 6(b) shows. So while the small component of the mixture can impart order onto the configuration of the large component, in the case that it alone interacts with the external potential, the large component does not succeed in passing down order onto the small component in the reverse case.

B. LID

Introducing small particles into a monodisperse system of large particles breaks the spanning network of large particles.

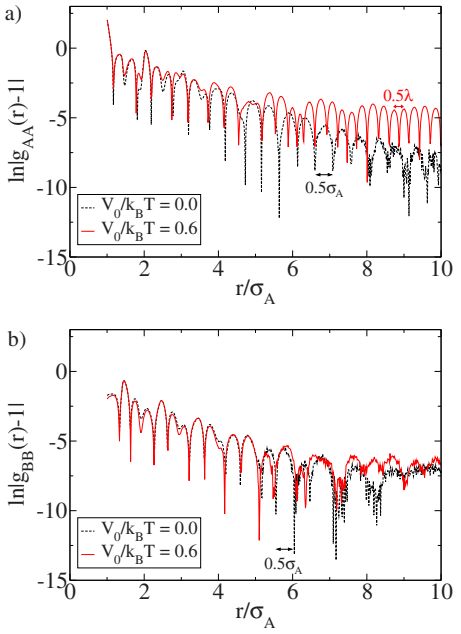

FIG. 6. (Color online) Comparison of the total pair correlation functions (a) $h_{AA}(r)$ and (b) $h_{BB}(r)$ of an equimolar mixture with $\sigma_B/\sigma_A=0.414$ exposed to an external, periodic potential at $\varrho^*=1.60$. Shown is the case when only the large component of the mixture interacts with the external potential.

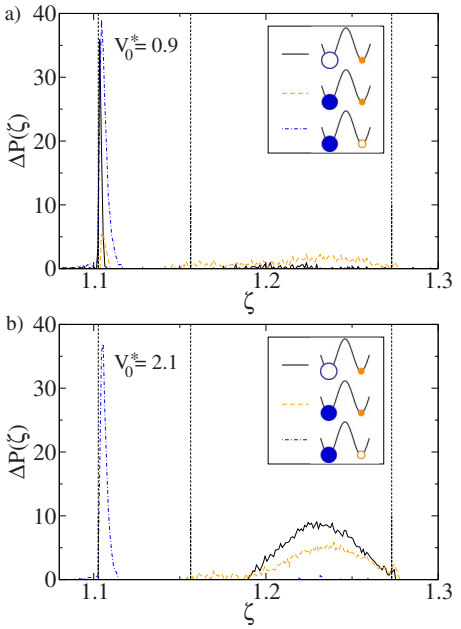

FIG. 7. (Color online) The change in the probability distribution of the shape factor $\Delta P(\zeta)$ for the different scenarios of coupling to the external field of the components of the mixture at $\varrho^*=1.71$. The coupling of a component to the external field is indicated in the schematic inset by a filled circle, while an open circle denotes no coupling to the external field of the component concerned. (a) All three cases are in the demixing regime for $V_0^*=0.9$. (b) At $V_0^*=2.1$ systems with a coupling of the small components to the external field have switched into the coexistence regime of the square lattice with the modulated liquid.

This results in a competition between free volume and configurational entropy and leads to clustering [41] and structural crossover [38–40]. Nevertheless in a purely repulsive system the effect is too weak to drive phase separation. A heuristic argument by Buhot *et al.* [42] yields a diameter ratio of $\sigma_B/\sigma_A=1/100$ as upper limit for possible phase separation in binary hard-disk mixtures. In the presence of a modulated external field the situation changes. For a given external potential the system will try to minimize its energy by aligning those components of the mixture with the potential minima that interact with the external field. If only one of the components interacts with the external field, one would therefore expect to observe a complete phase separation in an open boundary system. In the *NVT* ensemble by contrast this minimization of the energy competes with a maximization of entropy by an optimal packing of the hard-disks. This competition results in an ordering transition for dense systems. At low amplitudes V_0^* of the external field LID occurs [30,37]. Laser induced demixing results in the coexistence of a small component enriched fluid with a droplet of a monodisperse crystalline structure formed by the larger component for all the studied scenarios of coupling of the components of the mixture to the external field [37].

If only the smaller component of the mixture couples to the external field, this component will attempt to form chains along the minima of the external potential. Due to the chosen periodicity small particles on adjacent minima are uncoupled. This chain formation has a lower number density than the fluid mixture. Under the constraint of a fixed overall number density, the larger component is thus indirectly induced to form a dense packing, i.e., a triangular lattice structure in order to facilitate the energy minimization of the smaller components. Laser induced demixing takes place. As the large particles do not interact with the external potential, the crystallographic orientation of the droplet is arbitrary.

If in addition the larger component interacts with the external potential, these particles will also have to align with the potential minima in order to minimize the energy of the system. Large particles in adjacent minima will overlap, so a chain formation of large particles is not possible. A monodisperse triangular lattice of the large particles is not commensurate to the periodicity of the external field, instead a rhombic, commensurate lattice structure results. So also in this case a laser induced demixing occurs, although the underlying ordering mechanism and the resulting ordered structure differ from the first scenario.

In case that only the large component of the mixture is coupled to the external potential, no chain formation of the small component will take place. The system minimizes its energy solely by aligning the large particles with the potential minima and only the overall density induces the formation of rhombic, commensurate lattice structures in order to maximize entropy. Nevertheless this also results in a laser induced demixing.

The differences in the induced demixing show in the change in the probability distribution of the shape factor $\Delta P(\zeta)=P(\zeta;V_0^*)-P(\zeta;V_0^*=0.0)$ for the three scenarios of coupling to the external potential plotted in Fig. 7 for mixtures with $\varrho^*=1.71$. Systems with an interaction of the large component to the external field show a broader maximum

near $\zeta=1.1026$ than the system with exclusive interaction of the small component with the external potential. This is due to the fact that the Voronoi cells of the phase separated monodisperse, rhombic crystallites are not regular hexagonal cells. The range in potential strength V_0^* over which laser induced demixing is observed also differs for the various coupling scenarios. As shown in Fig. 7(b) at $V_0^*=2.1$ the systems with an interaction of the small component to the external field have already left the demixing regime. They show the characteristic broad maxima near $\zeta=1.273$, which are typical for the Voronoi cells in the $S_1(AB)$ square lattice. In addition the maxima in $\zeta=1.1026$ due to hexagonal Voronoi cells have disappeared completely. In contrast to this the system with exclusive interaction of the large component with the external field shows no tendency at all to form square lattice structures.

C. Fissuring regime

For all three scenarios of coupling the components of the mixture to the external potential at high densities only the commensurate $S_1(AB)$ square lattice structure allows for an energy minimization by aligning the relevant component to the potential minima and maximizing the entropy by a close packing. Therefore a laser induced freezing transition is expected to result in a $S_1(AB)$ Locked Floating Solid. In the monodisperse laser induced freezing scenario with a commensurate external potential, the resulting locked floating solid is stabilized solely by fluctuations. In contrast to this the geometry of the bidisperse system exposed to an external field commensurate to a $S_1(AB)$ square lattice structure provides a permanent coupling between adjacent minima at intermediate and high number densities ϱ^*, as the diameter of the large component σ_A is larger than the wavelength $\lambda=1/\sqrt{2}\varrho^*$ of the modulation in the commensurate case. A complete decoupling of adjacent minima occurs only for $\lambda \geq \frac{1}{2}(\sigma_A+\sigma_B)$, i.e., at densities below $\varrho^* \approx 1.0$. The system is geometrically blocked and a laser induced melting along the potential minima cannot occur. Nevertheless at high amplitudes V_0^* of the external potential, the position fluctuations show a pronounced anisotropy, which opens up a pathway to a different melting mechanism. Fluctuations in particle positions are enhanced along the minima of the external potential. Due to this, gaps in the sublattice of the large particles can form, which can be occupied by a small particle. In this way small particles can escape the cage formed by large particles and the sublattice of the smaller component starts to melt *along* the direction of the modulation. This leads to the formation of fissures in the sublattice of the larger component perpendicular to the minima of the external field, which are filled by the smaller component. For a commensurate choice of the modulation of the external potential (i.e., $\lambda=1/\sqrt{2}\varrho^*$), one can calculate the density at which a local fluctuation of the large particles will open up a large enough gap for a small particle to escape its cage. For the mixture under study this can occur for $\varrho^* \leq 1.56$. In the simulations fissuring sets in at far higher densities. This is due to long wavelength excitations in the crystal. The characteristics of the observed fissures also differ for the three simulated coupling scenarios of the components of the mixture to the external field. Systems, in which the small component interacts directly with the external potential, show the formation of dimers of small particles in the fissure that are oriented along the minima of the external potential, while for an exclusive interaction of the large component with the external potential the positions of the small particles within the fissures are arbitrary. As illustration Fig. 8 shows details of snapshots containing a fissure for the two different cases. The range of densities ϱ^* or alternatively packing fractions η over which the fissuring regime extends is larger for the case that both components interact with the external potential (phase diagram Fig. 10), than if only the smaller component couples to the external field (phase diagram Fig. 9 [30]).

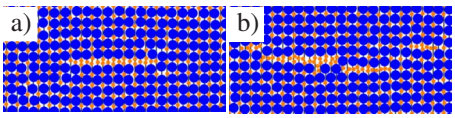

FIG. 8. (Color online) Detail of configurations containing a fissure in the $S_1(AB)$ square lattice, which forms in the presence of an external, one-dimensional modulated potential at $\varrho^*=1.73$ and $V_0^*=5.0$. (a) A typical fissure for the case, that only the small component interacts with the external potential. Small particles filling the fissure form dimers that orient along the minima of the external potential. (b) The situation for the case that only the large component of the mixture interacts with the external field. The placement of the small particles within the fissure is arbitrary.

D. LIF

In binary mixtures the geometric blocking of the laser induced melting transition, as it occurs in monodisperse systems, enhances the stabilization of the Locked Floating Solid by the external potential and leads e.g., to the occurrence of a coexistence between the locked floating solid and the modulated liquid for the case, that only the small component couple to the external field. This type of coupling to the

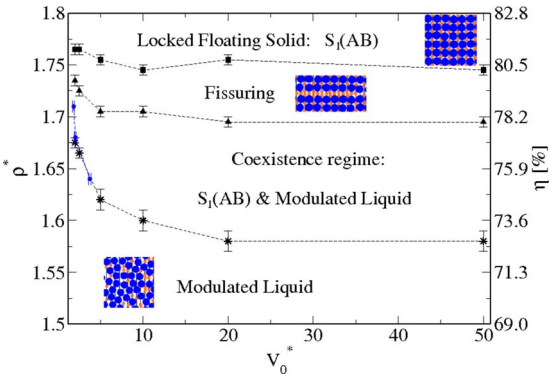

FIG. 9. (Color online) The phase diagram as obtained from the analysis of the order parameters S_B and S_A and the shape factor ζ for an equimolar binary mixture with diameter ratio $\sigma_B/\sigma_A=0.414$ exposed to an external periodic potential, commensurate to the $S_1(AB)$ square lattice for the case that only the small component of the mixture interacts with the external potential. Lines are a guide for the eyes. Figure reprinted from Franzrahe *et al.* [30], Fig. 4.

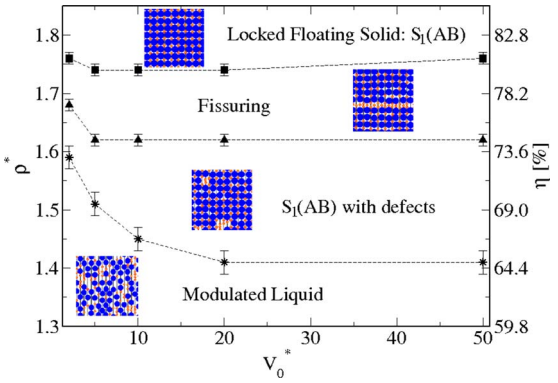

FIG. 10. (Color online) The phase diagram as obtained from the analysis of the order parameters S_B and S_A and the shape factor ζ for an equimolar binary mixture with diameter ratio $\sigma_B/\sigma_A=0.414$ exposed to an external periodic potential, commensurate to the $S_1(AB)$ square lattice for the case that both components of the mixture interact with the external potential. For this case of coupling to the external potential no laser induced coexistence occurs, but the fissuring regime and the $S_1(AB)$ lattice with defects are stabilized down to far lower packing fractions η as compared to the case, when only the small component interacts with the external potential (Fig. 9). Lines are a guide for the eyes.

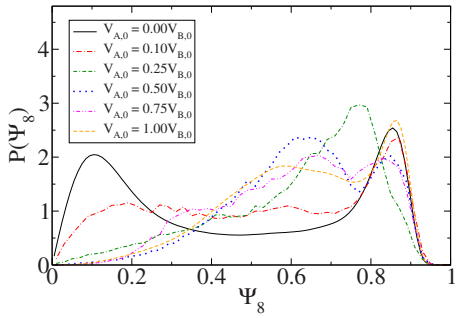

FIG. 11. (Color online) Probability distributions of the rotational order parameter Ψ_8 for various simulated strengths of coupling to the external field for the large component of the binary mixture at $\varrho^*=1.68$ and $V^*_{B,0}=V^*_0=2.1$.

external field results at intermediate to high external field amplitudes V_0^* in the existence of a $S_1(AB)$ square lattice locked floating solid at high densities ϱ^*, followed by a fissuring regime and a coexistence regime as the density decreases. At low densities the fluid phase is a modulated liquid. For a detailed discussion of the phase diagram, which is shown in Fig. 9 for this case, see [30].

The phase diagram for the situation, when both components of the mixture interact with the modulated, external field shown in Fig. 10, differs significantly from the one before in that there is no regime of coexistence between the $S_1(AB)$ lattice and the equimolar modulated liquid. An increase in the amplitude of the external potential at constant density leads to a competition between rhombic, monodisperse domains of the large component and square lattice domains. As the rhombic domains are directly stabilized by the external potential, these structures hamper the growth of the square lattice domain. The resulting lattice structure is a $S_1(AB)$ square lattice with frozen in disorder. Some of the disorder anneals with a further increase in V_0^*, but some defects and grain boundaries persist. As a comparison of the phase diagrams (compare Figs. 9 and 10) for the two discussed coupling scenarios shows, both phase boundaries, the one from the fissuring regime to the $S_1(A)$ lattice with frozen in disorder and the one to the modulated liquid, are shifted to considerably lower packing fractions for the case that both components of the mixture couple to the external potential. This is due to the direct stabilization by the external field of the occurring ordered phases. The phase diagram was calculated from simulation runs at constant V_0^* by lowering successively the density ϱ^* and adjusting the modulation of the external field. From an analysis of the probability distributions $P(S_B)$ and $P(S_A)$ the boundaries of the fissuring regime were obtained. The transition from the $S_1(AB)$ square lattice structure with frozen in disorder to the modulated liquid is difficult to determine. The lattice structure fragmentates into more and more competing domains as the number density ϱ^* decreases. In the phase diagram that density ϱ^* is shown as phase boundary, at which the probability distributions of the rotational order parameters Ψ_4 and Ψ_8 show a significant change. This is consistent with the fact that at these densities also $\langle S_B\rangle$ starts to grow monotonously, as the chain formation of the smaller component dominates.

From these studies it is evident that, if the large component also interacts with the external potential, it gets difficult to grow a perfect, defect free $S_1(AB)$ square lattice. So the question arises, up to which strength of coupling to the external field of the large component relative to that of the small component a coexistence between $S_1(AB)$ square lattice and modulated liquid does occur. For a comparison simulations at $\varrho^*=1.68$ with a coupling strength of $V^*_{B,0}=V^*_0$ of the smaller component to the external field were run with various strength of coupling for the large component: $V^*_{A,0}=0.0\cdot V^*_{0,B}$, $V^*_{A,0}=0.1\cdot V^*_{0,B}$, $V^*_{A,0}=0.25\cdot V^*_{0,B}$, $V^*_{A,0}=0.5\cdot V^*_{0,B}$, $V^*_{A,0}=0.75\cdot V^*_{0,B}$, and $V^*_{A,0}=1.0\cdot V^*_{0,B}$. In these simulations the amplitude V_0^* of the external potential was successively increased. It was found, that an additional coupling of the large component to the external field suppresses laser induced demixing and the condensation of a monodisperse, triangular lattice at small relative coupling strengths. The coupling strength for the larger component has to be above a threshold ($V^*_{A,0}>0.1\cdot V^*_{0,B}$) in order to induce a phase separation. The resulting monodisperse structure is rhombic due to the direct interaction of the large component with the external potential. At intermediate potential amplitudes V_0^* the differences in the laser induced freezing scenarios becomes apparent in the probability distributions of the rotational order parameter Ψ_8. The order parameter was evaluated in sub-boxes of the linear dimension $L_B=L/9$. Testing for an eightfold symmetry axis small and large particles in the system were considered. The resulting distributions $P(\Psi_8)$ for the simulated strengths of coupling to the external field for the large component are shown in Fig. 11 for $V_0^*=2.1$. These distributions show, that a coexistence of the $S_1(AB)$ square lattice with the modulated liquid occurs for $V^*_{A,0}<0.25\cdot V^*_{0,B}$. As the coupling of the large particles to the external field gets stronger the peak of the disordered phase disappears and the peak of the ordered phase gets broader. In

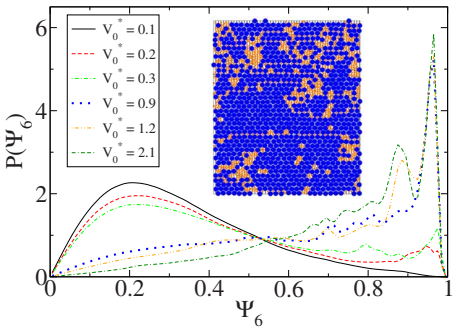

FIG. 12. (Color online) The probability distributions of the rotational order parameter Ψ_6 evaluated only with respect to the positions of the large particles show a substructure due to the grain boundaries and defects in the irregular monodisperse, rhombic crystal, but no tendency of the system to show a laser induced freezing transition into the commensurate $S_1(AB)$ square lattice locked floating solid.

conclusion, the weaker the coupling of the large component to the external field, the less defects hinder the growth of the $S_1(AB)$ square lattice.

For the case that exclusively the large component interacts with the external field *no* Laser Induced Freezing into a square lattice was observed in the simulations. Low potential strengths lead to a laser induced demixing into a monodisperse, rhombic crystal of the large component and a modulated liquid. As the potential amplitude V_0^* is raised no tendency to form square lattice structures was found in this system. Instead an irregular rhombic lattice with grain boundaries of the large component grows. The small particles fill the holes of this irregular crystal. A typical configuration is shown as an inset in Fig. 12. The probability distribution of the rotational order parameter Ψ_6 calculated from the configurations of the large component only, as they are shown in Fig. 12, are peaked near $\Psi_6=1$, but show a substructure due to the grain-boundaries. The simulations with varying relative coupling strength $V_{0,A}^*/V_{0,B}^*$ to the external field of the two components of the mixture already showed, that any coupling of the large component to the external field hinders the breaking up of the monodisperse, rhombic structures and the defect-free growth of square lattice structures. A restructuring of the rhombic crystallites into a square lattice at high densities is therefore rather improbable and the danger of getting stuck in a local minimum of the free energy is high in this system. So as for low number densities, in the Modulated Liquid phase, the exclusive coupling of the large component to the external field does not suffice to imprint order onto the small component of the mixture.

E. Commensurability of the external field

So far the phase behavior of a binary mixture in a modulated external field commensurate to the $S_1(AB)$ square lattice was analyzed. This raises the question, whether the laser induced phenomena discussed above do only occur in a commensurate setting. For a comparison the phase diagram for four incommensurate settings with constant, slightly different wavelengths ($\lambda=0.536$, $\lambda=0.541$, $\lambda=0.546$ and $\lambda=0.549$) of the external potential were calculated from Monte Carlo simulations. Only the small component was allowed to interact with the external potential. In these simulations a change in density can only be achieved by varying the length of the simulation box L_y and keeping L_x constant. Thus the starting configuration of the locked floating solid is a rectangular lattice structure at high densities instead of the square lattice structure of the previous studies. The differences in the locked floating solid is also apparent in the pair correlation functions $g_{BB}(\vec{r})$ and $g_{AA}(\vec{r})$. These are plotted in Fig. 13 for $V_0^*=5.0$ for two number densities ϱ^* for systems with a constant wavelength $\lambda=0.546$ of the periodic external potential. The anisotropy in the maxima of $g_{BB}(\vec{r})$ reflects clearly the coupling of the small particles to the external potential at both number densities. As the large particles do not couple to the external potential directly, isotropic maxima in the pair correlation function $g_{AA}(\vec{r})$ are to be expected. Nevertheless due to the structure of the locked floating solid in these incommensurate settings the maxima of $g_{AA}(\vec{r})$ show a strong anisotropy at high number densities. Here fluctuations of the large particles along the minima of the external potential are suppressed. Only at lower number densities, as the locked floating solid approaches a square lattice structure, do the maxima in $g_{AA}(\vec{r})$ get isotropic.

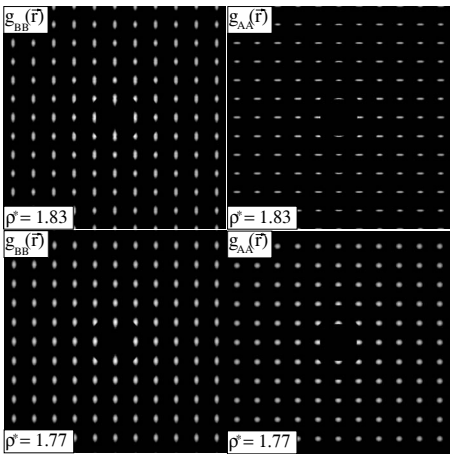

FIG. 13. Pair correlation functions $g_{BB}(\vec{r})$ and $g_{AA}(\vec{r})$ for a binary mixture exposed to an incommensurate, periodic external potential with $\lambda=0.546$ and $V_0^*=5.0$ at two different number densities ϱ^*.

An analysis of the order parameters S_A and S_B as well as of the shape factor ζ was used for the calculation of the phase diagram from the incommensurable simulations. An overlay of the phase boundaries for all four systems is given in Fig. 14. These phase diagrams intersect the plane of commensurability consistently. The wavelengths $\lambda=0.536$ and $\lambda=0.541$ correspond to the commensurate densities $\varrho^*=1.74$ and $\varrho^*=1.71$. At these densities the system is in the fissuring regime. The other two wavelengths correspond to densities ($\lambda=0.546$ to $\varrho^*=1.68$ and $\lambda=0.549$ to $\varrho^*=1.66$) at which the system is in the coexistence regime of the $S_1(AB)$ square lattice and the modulated liquid. The existence of a locked floating solid, a fissuring regime and a coexistence region could be confirmed for incommensurate settings from these simulations. But due to the incommensurability with

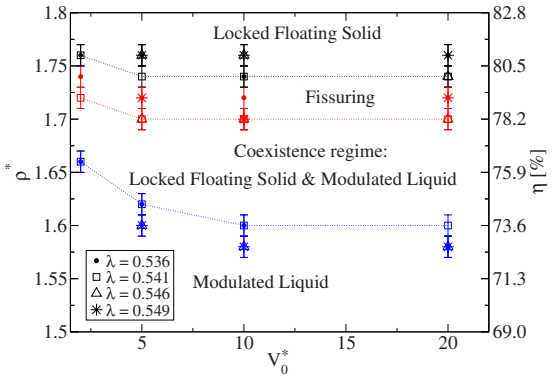

FIG. 14. (Color online) The phase diagrams as obtained from the analysis of the order parameters S_B and S_A and the shape factor ζ for an equimolar binary mixture with diameter ratio $\sigma_B/\sigma_A=0.414$ exposed to external periodic potentials, *in*commensurate to the $S_1(AB)$ square lattice for the case that only the small component of the mixture interacts with the external potential. Lines are a guide for the eyes.

the $S_1(AB)$ square lattice, the crystallographic characteristics of the locked floating solid differ. They change from a rectangular oriented with its long axis perpendicular to the potential minima at high number densities to one oriented along the potential minima at densities below the commensurate density for a given wavelength. The simulations showed furthermore that at high densities and intermediate amplitudes of the external potential V_0^* the rectangular locked floating solid can be unstable against the occurrence of fractures. Unlike the fissures at lower densities the fractures run in diagonals through the crystal and will heal again as the density is lowered. From these studies one can conclude, that for an experimental realization with a fixed wavelength for the external light field, a wavelength that intersects the plane of commensurability in the coexistence regime should be chosen in order to enable the observation of all laser induced phenomena.

F. Importance of the packing fraction of the mixture

The phase diagrams discussed for the various coupling scenarios for the components of the binary mixture are not only given in terms of number density ϱ^* as a function of the amplitude of the external potential, but also in terms of the packing fraction η. This is a more general variable for binary mixtures, as mixtures deviating from an equimolar mixture or with different diameter ratios can have the same packing fraction as the so far studied equimolar binary mixture with $\sigma_B/\sigma_A=0.414$. Therefore the influence of deviations in the concentration of large particles from $x_A=50\%$ on the phase diagram for a system with exclusive interaction of the smaller component with the external field was studied. The reference system for the comparison is the equimolar mixture with $\sigma_B/\sigma_A=0.414$ at $\varrho^*=1.71$. Thus the packing fraction is $\eta=78.7\%$. At this packing fraction an increase of the amplitude of the external potential induces first a demixing and results at higher amplitudes in a coexistence of the square lattice with the modulated liquid. A lowering of the concentration of large particles in the mixture by approximately 3% ($x_A=46.9\%$) lowers the packing fraction to only $\eta=75.2\%$. At this packing fraction the phase diagram for the equimolar mixture (Fig. 9) suggest that no demixing should occur before the coexistence regime is reached as V_0^* is increased. This is confirmed by simulations. Figure 15(a) shows the change in the probability distributions of the shape factor ζ with respect to the probability distribution at $V_0^*=0.0$, i.e., $\Delta P(\zeta)=P(\zeta;V_0^*)-P(\zeta;V_0^*=0.0)$, for the mixture with $x_A=46.9\%$. For the reference mixture with $x_A=50.0\%$ $\Delta P(\zeta)$ is depicted in Fig. 15(b). In contrast to the equimolar mixture the $x_A=46.9\%$ mixture shows no enhancement of the peak for regular, hexagonal Voronoi cells in $\Delta P(\zeta)$ at low V_0^*, i.e., laser induced demixing. The mixture shows instead a direct transition to the coexistence regime. An increase in the concentration of large particles to $x_A=53.1\%$ in contrast increases the packing fraction to $\eta=82.1\%$ at a number density of $\varrho^*=1.71$. At such high pack-

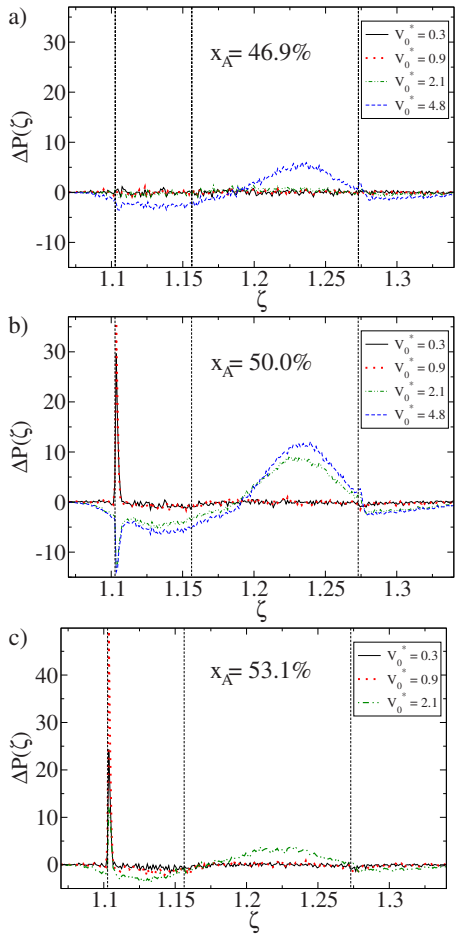

FIG. 15. (Color online) The change in the probability distributions of the shape factor ζ at various amplitudes of the external potential V_0^* with respect to the probability distribution at $V_0^*=0.0$ for a binary mixtures with diameter ratio $\sigma_B/\sigma_A=0.414$ with exclusive coupling of the small particles to the external potential is plotted for mixtures with various concentrations of large particles x_A. (a) At $x_A=46.9\%$ and a number density of $\varrho^*=1.71$ the mixture has a packing fraction of $\eta=75.2\%$. (b) The reference mixture with $x_A=50.0\%$ at $\varrho^*=1.71$ has a packing fraction of $\eta=78.7\%$ as has the mixture with $x_A=53.1\%$ in (c) at $\varrho^*=1.64$.

ing fractions the reference mixture is already in the ordered phase. This hampers a direct comparison with the reference system. Instead this mixture was simulated at $\varrho^*=1.64$ which corresponds to $\eta=78.7\%$, which is the same packing fraction as the reference mixture has. So one expects to observe, demixing followed by coexistence as V_0^* is increased. In Fig. 15(c) $\Delta P(\zeta)$ for the mixture with $x_A=53.1\%$ is plotted. For this case the peak for regular, hexagonal Voronoi cells is enhanced in comparison to the reference mixture shown in Fig. 15(b). The monodisperse crystallite does not dissolve as easily, so at $V_0=2.1$ there is still a peak in $\Delta P(\zeta)$ at $\zeta=1.1026$ due to regular, hexagonal Voronoi cells. Nevertheless square lattice structures have already formed, as can be seen by the broad maximum that has developed near $\zeta=1.273$.

Deviations in the ratio of diameter from $\sigma_B/\sigma_A=0.414$ in an equimolar mixture will also result in changes in the packing fraction η. As a reference the equimolar system with $\sigma_B/\sigma_A=0.414$ at $\varrho^*=1.71$ with only the smaller component interacting with the external field was taken. Simulations at the same number density and with diameter ratios $\sigma_B/\sigma_A=0.154$, 0.300, 0.400, 0.420, and 0.430 with a successive increase in V_0^* were conducted. For $\sigma_B/\sigma_A=0.154$ the densest packing can be achieved by a triangular lattice of the large component with small particles placed in the interstices of this lattice. Such a structure is not commensurate to the external, periodic field. At the density of choice, $\varrho^*=1.71$, the commensurate $S_1(AB)$ square lattice structure can accommodate small particles of up to a diameter of $\sigma_B=0.529$ in the interstices of the square lattice of large particles without an overlap. The maximum diameter of small particles used in simulations for the comparison of the phase behavior as the amplitude of the external potential is increased, is $\sigma_B=0.430$. With this choice of simulated mixtures the range of packing fractions analyzed is 68.7%–79.6%. Figure 16 shows $\Delta P(\zeta)$, the change in the probability distributions for these mixtures with respect to the corresponding field free cases with $V_0^*=0$, for the simulated ratio of diameter at various potential strengths V_0^*. At low amplitudes of the external potential, as shown in Fig. 16(a), only mixtures with $\sigma_B \geq 0.414$ show the typical peak for regular, hexagonal Voronoi cells at $\zeta=1.1026$, which signifies laser induced demixing. The packing fractions of the remaining mixtures are too low to show any demixing at $V_0^*=0.3$. While the mixture with $\sigma_B=0.400$ shows demixing at $V_0^*=0.9$, no change in the structure of the Voronoi cells is induced for the mixtures with $\sigma_B/\sigma_A=0.154$ and 0.300. This is consistent with the phase behavior of the reference mixture (Fig. 9). The mixture with $\sigma_B=0.414$ shows laser induced demixing at low V_0^* only for packing fraction $\eta>75\%$. At the given number density the mixtures with $\sigma_B \leq 0.300$ lie below this limit. For $V_0^*=2.1$ as shown in Fig. 16(c) the reference mixture with $\sigma_B=0.414$ is in the coexistence regime. In this regime the difference between systems with diameter ratios smaller than the reference system and those with larger ratios can be discerned. While the mixture with $\sigma_B=0.400$ shows an analogous behavior as the reference mixture, the systems with larger ratio of diameter still show a significant fraction of Voronoi cells with regular, hexagonal structure in the configurations. In such mixtures due to their higher packing fraction η the monodisperse, triangular lattice crystallites cannot dissolve easily. The mixtures with $\sigma_B/\sigma_A=0.154$ and 0.300 show no significant change in the distribution of the shape factor for these amplitudes of the external potential. For $\sigma_B=0.300$ the mixture has a packing fraction $\eta=73.2\%$. The phase diagram of the reference mixture in Fig. 9 shows that the transition line between coexistence regime and modulated liquid for high amplitudes of the external potential V_0^* lies in the region of $\varrho^* \approx 1.59$, i.e., $\eta \approx 73.1\%$. The mixture with $\sigma_B=0.300$ lies with its packing fraction within this transition region at high V_0^*. Simulations for this mixture up to $V_0^*=8.4$ showed a slight increase in the local fourfold rotational order, but a transition into the coexistence regime did not occur.

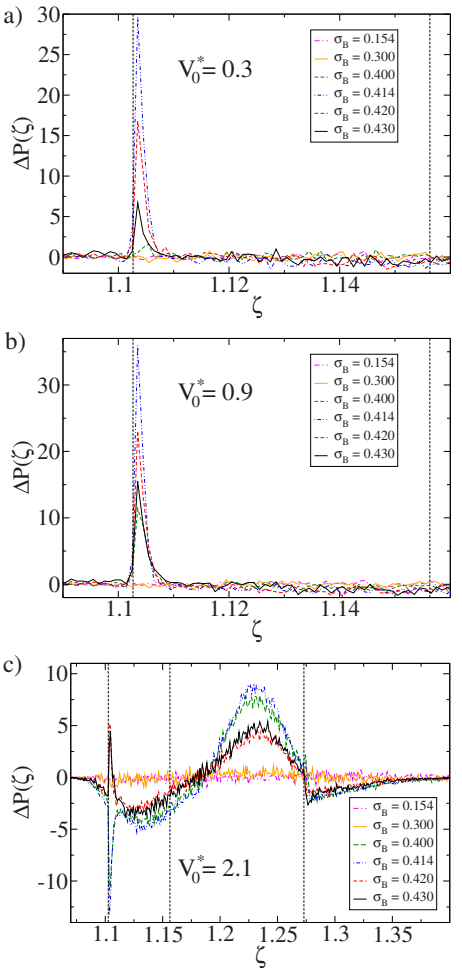

FIG. 16. (Color online) The change in the probability distributions of the shape factor ζ at various amplitudes of the external potential V_0^* with respect to the probability distribution at $V_0^*=0.0$ for equimolar, binary mixtures with exclusive coupling of the small particles to the external potential is plotted for mixtures with various diameter ratios σ_B/σ_A. Shown are the distributions in the demixing regime of the reference mixture at (a) $V_0^*=0.3$ and (b) $V_0^*=0.9$ and in the coexistence regime of the square lattice with the modulated liquid of the reference mixture at (c) $V_0^*=2.1$.

V. CONCLUSIONS

We have shown via Monte Carlo simulations that complex lattice structures in binary hard-disk mixtures form ther-

modynamically stable phases only in a high pressure environment. An alternative, successful route to the controlled structuring of such binary mixtures is exposing the system to a modulated external field. Weak external fields allow a controlled tuning of the miscibility of the mixture. The ordering mechanisms resulting in a laser induced demixing (LID) in this regime depends on the details of the coupling of the components of the mixture to the modulating field. Also the occurrence of laser induced freezing and the existence of a coexistence between the $S_1(AB)$ square lattice and the modulated liquid was shown to depend strongly on the details of the coupling of the components of the mixture to the external, modulating field. On the other hand slight deviations from the characteristics of the system as the concentration of large particles x_A or the diameter ratio σ_B/σ_A, as they are probable to occur in any experimental realization, could be shown to have no impact on the occurrence of the laser induced phenomena, as long as the mixtures stays in the relevant range of packing fraction η. This was also shown to be true for slight deviations from the constraint of commensurability of the periodicity of the external potential with respect to the $S_1(AB)$ square lattice.

ACKNOWLEDGMENTS

This work was funded by the Deutsche Forschungsgesellschaft (Grant No. SFB TR6/C4). Granting of computer time from HLRS, NIC, and SSP is gratefully acknowledged.

[1] A. van Blaaderen, R. Ruel, and P. Wiltzius, Nature (London) **385**, 321 (1997).
[2] M. Allard, E. Sargent, P. Lewis, and E. Kumacheva, Adv. Mater. **16**, 1360 (2004).
[3] M. H. Kim, S. H. Im, and O. O. Park, Adv. Mater. **17**, 2501 (2005).
[4] Q. Yan, X. F. Ang, C. C. Wong, and Y.-M. Chiang, Appl. Phys. A **94**, 271 (2009).
[5] Y.-H. Cho, G. Cho, and J.-S. Lee, Adv. Mater. **16**, 1814 (2004).
[6] J. C. Crocker and D. G. Grier, J. Colloid Interface Sci. **179**, 298 (1996).
[7] P. Habdas and E. R. Weeks, Curr. Opin. Colloid Interface Sci. **7**, 196 (2002).
[8] A. Chowdhury, B. J. Ackerson, and N. A. Clark, Phys. Rev. Lett. **55**, 833 (1985).
[9] K. Loudiyi and B. Ackerson, Physica A **184**, 1 (1992).
[10] K. Loudiyi and B. Ackerson, Physica A **184**, 26 (1992).
[11] J. Chakrabarti, H. R. Krishnamurthy, and A. K. Sood, Phys. Rev. Lett. **73**, 2923 (1994).
[12] J. Chakrabarti, H. R. Krishnamurthy, A. K. Sood, and S. Sengupta, Phys. Rev. Lett. **75**, 2232 (1995).
[13] Q.-H. Wei, C. Bechinger, D. Rudhardt, and P. Leiderer, Phys. Rev. Lett. **81**, 2606 (1998).
[14] C. Bechinger, M. Brunner, and P. Leiderer, Phys. Rev. Lett. **86**, 930 (2001).
[15] E. Frey, D. R. Nelson, and L. Radzihovsky, Phys. Rev. Lett. **83**, 2977 (1999).
[16] L. Radzihovsky, E. Frey, and D. R. Nelson, Phys. Rev. E **63**, 031503 (2001).
[17] C. Bechinger and E. Frey, J. Phys.: Condens. Matter **13**, R321 (2001).
[18] W. Strepp, S. Sengupta, and P. Nielaba, Phys. Rev. E **63**, 046106 (2001).
[19] W. Strepp, S. Sengupta, and P. Nielaba, Phys. Rev. E **66**, 056109 (2002).
[20] P. Chaudhuri, C. Das, C. Dasgupta, H. R. Kirshnamurthy, and A. K. Sood, Phys. Rev. E **72**, 061404 (2005).
[21] D. Chaudhuri and S. Sengupta, Phys. Rev. E **73**, 011507 (2006).
[22] F. Bürzle and P. Nielaba, Phys. Rev. E **76**, 051112 (2007).
[23] K. J. Strandburg, Rev. Mod. Phys. **60**, 161 (1988).
[24] K. J. Strandburg, Rev. Mod. Phys. **61**, 747 (1989).
[25] K. Binder, S. Sengupta, and P. Nielaba, J. Phys.: Condens. Matter **14**, 2323 (2002).
[26] J. Zanghellini, P. Keim, and H. H. von Grünberg, J. Phys.: Condens. Matter **17**, S3579 (2005).
[27] H. H. von Grünberg, P. Keim, K. Zahn, and G. Maret, Phys. Rev. Lett. **93**, 255703 (2004).
[28] U. Gasser, G. Maret, and P. Keim, Phys. Unserer Zeit **39**, 36 (2008).
[29] C. N. Likos and C. L. Henley, Philos. Mag. B **68**, 85 (1993).
[30] K. Franzrahe and P. Nielaba, Phys. Rev. E **76**, 061503 (2007).
[31] N. Metropolis, A. W. Rosenbluth, M. N. Rosenbluth, A. H. Teller, and E. Teller, J. Chem. Phys. **21**, 1087 (1953).
[32] L. Lue and L. Woodcock, Mol. Phys. **96**, 1435 (1999).
[33] M. C. Jenkins and S. U. Egelhaaf, J. Phys.: Condens. Matter **20**, 404220 (2008).
[34] F. Moučka and I. Nezbeda, Phys. Rev. Lett. **94**, 040601 (2005).
[35] P. Chaikin and T. Lubensky, *Principles of Condensed Matter Physics* (Cambridge University Press, Cambridge, UK, 1995).
[36] I. Götze, J. Brader, M. Schmidt, and H. Löwen, Mol. Phys. **101**, 1651 (2003).
[37] K. Franzrahe, P. Nielaba, A. Ricci, K. Binder, S. Sengupta, P. Keim, and G. Maret, J. Phys.: Condens. Matter **20**, 404218 (2008).
[38] C. Grodon, M. Dijkstra, R. Evans, and R. Roth, J. Chem. Phys. **121**, 7869 (2004).
[39] C. Grodon, M. Dijkstra, R. Evans, and R. Roth, Mol. Phys. **103**, 3009 (2005).
[40] J. Baumgartl, R. P. A. Dullens, M. Dijkstra, R. Roth, and C. Bechinger, Phys. Rev. Lett. **98**, 198303 (2007).
[41] N. Hoffmann, F. Ebert, C. N. Likos, H. Löwen, and G. Maret, Phys. Rev. Lett. **97**, 078301 (2006).
[42] A. Buhot and W. Krauth, Phys. Rev. E **59**, 2939 (1999).